ADA046350

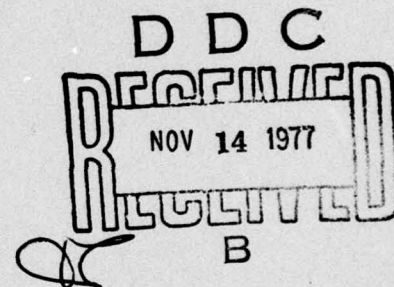(12)
B.S

Rapid Variations in Spacecraft Potential

H. B. GARRETT, CAPT, USAF
A.L. PAVEL. CAPT, USAF
D.A. HARDY, 1LT, USAF

DDC

RECEIVED

NOV 14 1977

B

6 June 1977

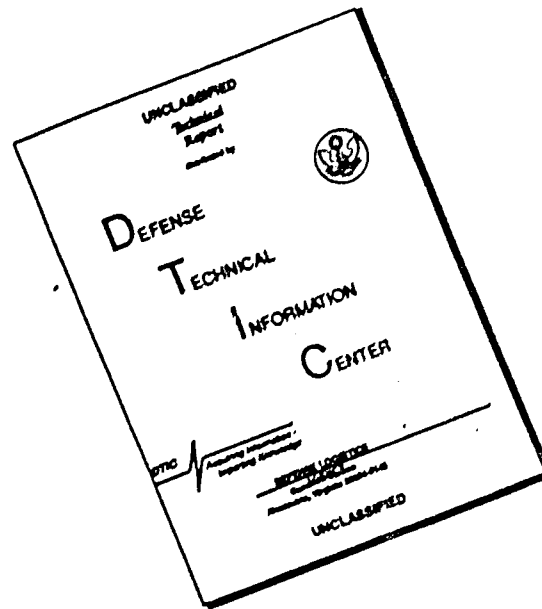AD No. _____
DDC FILE COPY

SPACE PHYSICS DIVISION   PROJECT 7661

AIR FORCE GEOPHYSICS LABORATORY

HANSCOM AFB, MASSACHUSETTS 01731

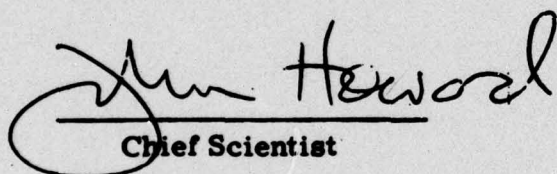# AIR FORCE SYSTEMS COMMAND, USAF

DISCLAIMER NOTICE

THIS DOCUMENT IS BEST QUALITY AVAILABLE. THE COPY FURNISHED TO DTIC CONTAINED A SIGNIFICANT NUMBER OF PAGES WHICH DO NOT REPRODUCE LEGIBLY.

This report has been reviewed by the ESD Information Office (OI) and is releasable to the National Technical Information Service (NTIS).

This technical report has been reviewed and is approved for publication.

FOR THE COMMANDER

Chief Scientist

Air Force surveys in geophysics

REPORT DOCUMENTATION PAGE	READ INSTRUCTIONS BEFORE COMPLETING FORM

1. REPORT NUMBER	2. GOVT ACCESSION NO.	3. RECIPIENT'S CATALOG NUMBER
AFGL-TR-77-0132	AFGL-AFSG-369	

4. TITLE (and Subtitle)	5. TYPE OF REPORT & PERIOD COVERED
RAPID VARIATIONS IN SPACECRAFT POTENTIAL	Scientific, Interim
	6. PERFORMING ORG. REPORT NUMBER
	AFSG, No. 369

7. AUTHOR(s)	8. CONTRACT OR GRANT NUMBER(s)
H. B. Garrett, Capt, USAF A. L. Pavel, Capt, USAF* D. A. Hardy, 1/Lt, USAF	

9. PERFORMING ORGANIZATION NAME AND ADDRESS	10. PROGRAM ELEMENT, PROJECT, TASK AREA & WORK UNIT NUMBERS
Air Force Geophysics Laboratory (PHG) Hanscom AFB, Massachusetts 01731	P 76610801 62101F

11. CONTROLLING OFFICE NAME AND ADDRESS	12. REPORT DATE
Air Force Geophysics Laboratory (PHG) Hanscom AFB, Massachusetts 01731	6 June 1977
	13. NUMBER OF PAGES
	42

14. MONITORING AGENCY NAME & ADDRESS(if different from Controlling Office)	15. SECURITY CLASS. (of this report)
40 p.	Unclassified
	15a. DECLASSIFICATION/DOWNGRADING SCHEDULE

16. DISTRIBUTION STATEMENT (of this Report)

Approved for public release; distribution unlimited.

D D C
RECEIVED
NOV 14 1977
B

17. DISTRIBUTION STATEMENT (of the abstract entered in Block 20, if different from Report)

18. SUPPLEMENTARY NOTES

*Edwards AFB, California

19. KEY WORDS (Continue on reverse side if necessary and identify by block number)

Spacecraft charging   Communications satellites
Spacecraft
Geosynchronous orbit environment
Spacecraft potential variations
Satellite anomalies

20. ABSTRACT (Continue on reverse side if necessary and identify by block number)

The increasing complexity and sophistication of synchronous orbit satellites has resulted in a corresponding increase in their susceptibility to anomalous behavior and disruption. Many of these problems can be attributed to the buildup of large potentials on various surfaces of the satellites in response to the ambient space plasma. Such large potentials (as great as -20,000 V relative to the ambient plasma) can produce anomalies and disruptions by causing arcing between the surfaces. In this report, the question of the time rate of change of satellite potential is studied. Theory and observations are reviewed

DD FORM 1 JAN 73 1473   EDITION OF 1 NOV 65 IS OBSOLETE

409 578

20.   (Cont) *from p (473A)*

to give estimates of the time rate of change in potentials encountered at synchronous orbit.   A clear need for future study is indicated.   Plans for instrumentation being developed at AFGL to study the area are discussed.

ACCESSION for

NTIS   White Section
DDC   Buff Section   ☐
UNANNOUNCED   ☐
JUSTIFICATION

BY
DISTRIBUTION/AVAILABILITY CODES
Dist.   AVAIL. and/or SPECIAL

A

Preface

Without many hours of discussion with Dr. DeForest of the University of California at San Diego, this report would have been impossible. His patient explanations were of crucial importance in understanding the ATS-5 and ATS-6 data. We are grateful to C. Pike of AFGL who spent several hours reviewing and correcting our manuscript. Valuable comments were contributed by Drs. Rubin and Rothwell of AFGL.

Contents

5

Illustrations

Tables

7

Rapid Variations in Spacecraft Potential

1. INTRODUCTION

The increasing complexity and sophistication of synchronous orbit satellites have increased their susceptibility to disruption and anomalous behavior. McPherson et al,[1] Shaw et al,[2] and Pike and Bunn[3] have demonstrated that many of these occurrences are related to changes in geomagnetic activity and geomagnetic substorms (see Figure 1) and are often the result of satellite potential variations. DeForest[4,5] has shown a definite connection between variations in spacecraft potential and plasma injection at geosynchronous orbit during substorms. Supporting these findings, Reasoner et al[6] have found an inverse correlation between spacecraft encounters with the low energy plasmasphere and spacecraft potential variations. Several workers (see, for example, Parker,[7] Whipple,[8] or Rothwell et al,[9]) have attempted to theoretically model the problem of computing the response of a spacecraft to a changing ambient plasma environment. Although a complete understanding of the spacecraft charging phenomenon is still lacking, all of these studies have contributed to rapid progress in defining the problem and in understanding the factors involved in the disruption and anomalous behavior of synchronous orbit satellites.

One area that has not been well defined in previous studies is that of the timescales over which variations in satellite potential take place. The time-rate of
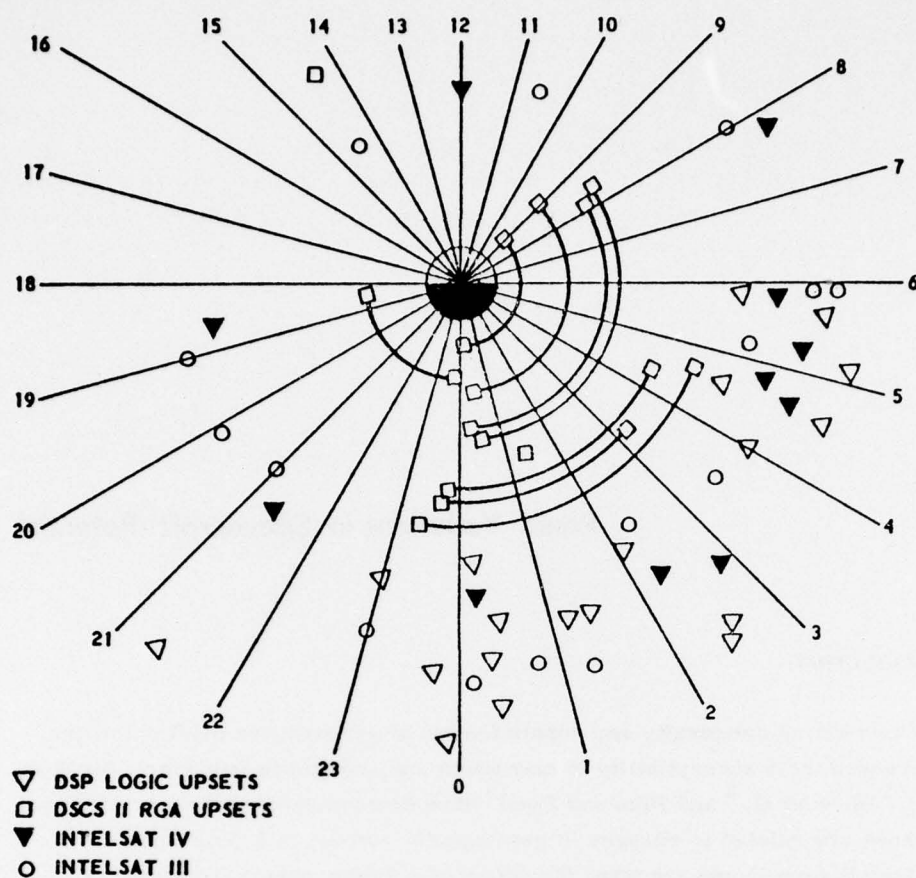
Figure 1. Local Time Plot of Various Satellite Disruptions and Anomalies.[1] The radial variations are not real but merely for graphical representation

change of satellite potential may have significant effect on the extent of differential charging on the satellite, the discharge rate, and the ultimate potential which the satellite reaches. To help in understanding these scales, this report summarizes and catalogs examples of the various types of charging that have been observed. The time-scales of the associated potential variations will be compared and tabulated to determine the extent to which such variations can cause problems for the spacecraft. In addition, we will estimate the order of magnitude of the charging rate and recommend areas of future study.

To provide a background for the study of spacecraft potential variations, we will begin by describing the geosynchronous environment and by presenting a static model of spacecraft charging that provides a qualitative explanation of charging

10

under various ambient conditions. Examples from the ATS-5 and ATS-6 geo-synchronous satellites will be used to illustrate the ambient plasma environment and its effect on the spacecraft potential. Similarly, the theory of time variations of spacecraft potential will be reviewed and ATS-5 and ATS-6 data used to provide estimates of the order of magnitude of the rate of change of the spacecraft potential. We will conclude with a description of problem areas and instrumentation designed specifically to study such time variations.

2. SYNCHRONOUS ENVIRONMENT

The synchronous orbit environment (6.62 earth radii from the center of the earth) is unique in the variability of the plasma and field characteristics encountered. Interior to synchronous orbit, the earth's magnetic field is sufficiently strong that it effectively dominates charged particle motion. Near synchronous orbit the collective kinetic energy of the ambient particles is sufficient to alter the constraining magnetic field and cause large variations in plasma conditions on a small time scale. The occurrence of rapid changes in plasma parameters associated with the injection of high temperature plasma into the synchronous orbit regime is the most important factor in spacecraft charging.

Figure 2 depicts the location of the synchronous orbit environment within the earth's magnetic field and the variability of conditions observed there. There are four distinct regions of plasma normally observed at the synchronous orbit. These regions are:

2.1 Plasmasphere

The plasmasphere is the region of the low energy relatively high density plasma which dominates the near earth region of the magnetosphere. It is essentially an extension of the earth's ionosphere. Its outer boundary is the plasmapause (P). Near synchronous orbit the plasmasphere is characterized by plasma densities of a few particles per cubic centimeter and plasma temperatures of a few electron volts. [10, 11] During the encounter of the plasmasphere by the ATS-6 satellite, the density was found to range between 1 to 10 ions per cm^3, with temperatures between 1 to 50 eV. [6] During a magnetospheric substorm the outer boundary of the plasmasphere or the plasmapause moves significantly earthward and this low energy plasma component is no longer observed at synchronous orbit.

10.   Frank, L. A. (1971) On the relationship of the plasma sheet, ring current trapping boundary, and plasmapause near the magnetic equator and local midnight, J. Geophys. Res., 76;(No. 10):2265.

11.   Gringauz, K. I. (1969) Low energy plasma in the earth's magnetosphere, Rev. Geophys., 7(No. 1, 2):339.
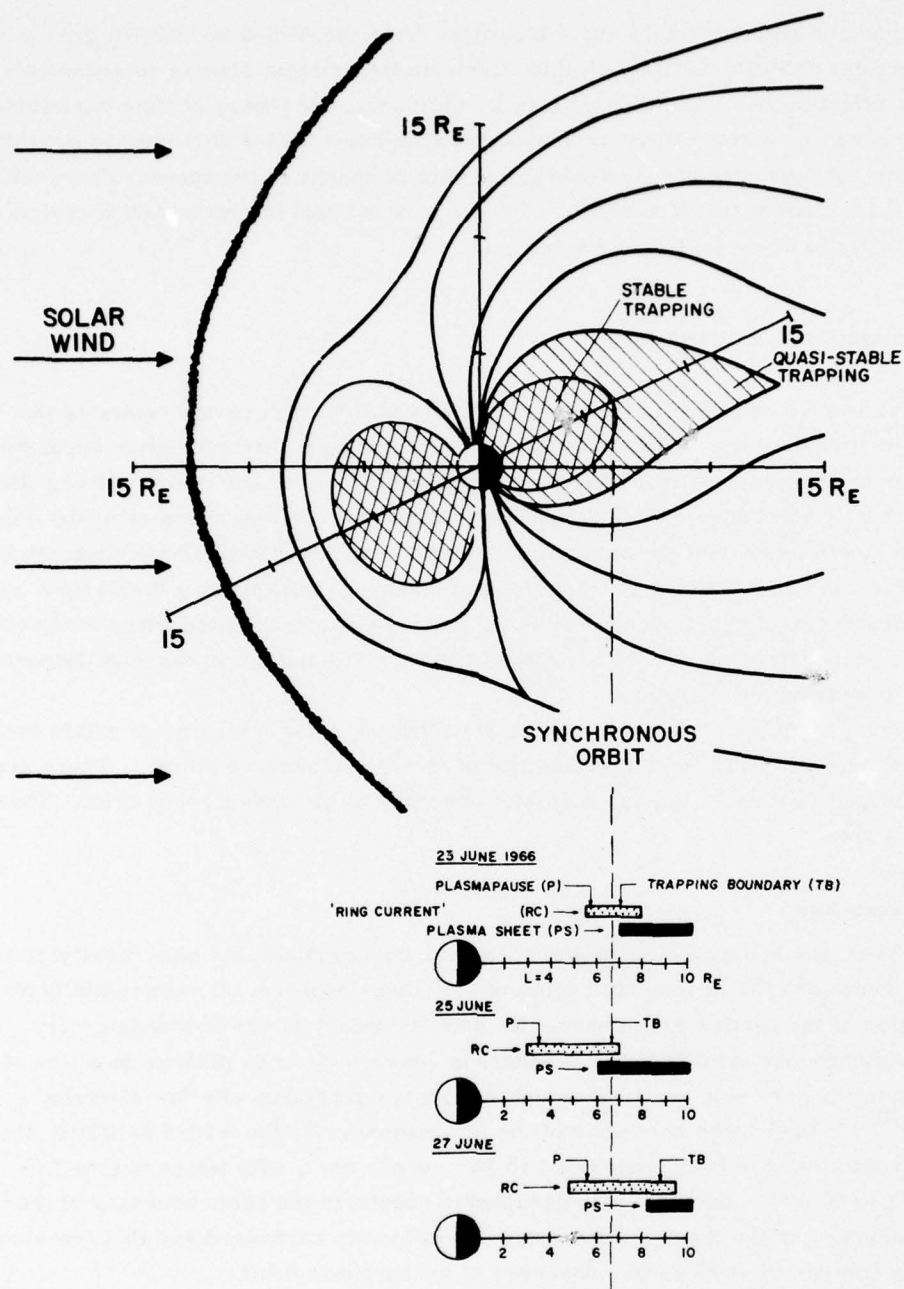
Figure 2. The Relative Locations of the Plasma Regions Dominating Sychronous
Orbit and Their Motion During Disturbed Geomagnetic Periods. The 25 June
diagram shows the earthward movement of the plasma sheet and plasmapause during
a substorm[10]

12

2.2 Ring Current (RC)

The ring current is a region of ions and electrons, elevated in temperature, that has densities on the order of the plasmapause.[12] Typical values of 1 per cm^3 and temperatures of 20 to 40 keV were determined from ATS-6 data. This component is almost always present at synchronous orbit near local midnight.

2.3 Trapping Boundary (TB)

The trapping boundary is the edge of the region of stably trapped particles (designated here for 40 keV electrons). This can be considered as the line of demarcation between those regions where particle motion is strongly under the influence of the earth's magnetic field and the regions where particle kinetic energy is the controlling factor. Within the trapping boundary, the fluxes of high energy particles (1 MeV or higher) can be defined and radiation dose rates determined with some degree of accuracy. Since a satellite in synchronous orbit is, except for periods of severe geomagnetic activity, within the trapping boundary, the radiation levels resulting from the high energy particle fluxes limit the long term survivability of the satellite.

2.4. Plasma Sheet (PS)

The plasma sheet comprises a high temperature plasma in the earth's magnetotail. Except when forced inward from the magnetotail during injection events, it remains beyond synchronous orbit. The plasma sheet particles have temperatures normally of several kiloelectron volts per particle, a value not high enough to constitute a substantial threat from the standpoint of radiation damage. However, during disturbed times these kiloelectron-volt plasma electrons are injected into the synchronous orbit forming the ring current. This is accompanied by the inward motion of the plasmapause such that no low energy plasma is present at the synchronous orbit. Such a situation can result in charging of spacecraft surfaces to potentials of several thousands volts.[4]

3. SATELLITE POTENTIAL VARIATIONS – TIME INDEPENDENT

3.1 Theory

The potential on a satellite immersed in a plasma will vary such that the sum of all currents to the satellite is zero. The primary contributors to this current balance are the ambient plasma electrons and ions, secondary electrons released from the surface by electron and ion impact, and photoelectrons released by solar

12. Hones, M. E., Jr. (1972) Plasma sheet variation during substorms, Planet. Space Sci., 20(No. 9):1409.

illumination of the satellite surface. Following the development given by Rosen,[13] a simple model will be discussed that demonstrates how the surface potential varies such that these currents balance to zero.

The neutral gas density at synchronous orbit is sufficiently small that collisional processes can be ignored. It will be assumed that the secondary electron current is small compared with the ambient electron current (J_e), ion current (J_i), and photoelectron current (J_{ph}), and thus can be ignored. At equilibrium, current balance requires:

$$J_e - J_i - J_{ph} = 0 \ . \tag{1}$$

During solar illumination, the ambient electrons and photoelectron currents so dominate the ion current that to first order:

$$J_e - J_{ph} = 0 \ . \tag{2}$$

Similarly, in the absence of illumination, the photoelectron current is zero and the current balance is given approximately by:

$$J_e - J_i = 0 \ . \tag{3}$$

The ambient electron flux will often dominate the ambient ion flux since, at comparable temperatures, the electrons will have a much greater velocity than the ions and, hence, a greater flux to the satellite surface. These conditions occur when the satellite is immersed in the plasma sheet during geomagnetic storms. The electron flux during such periods drives the spacecraft surface to a negative potential in order to repel the higher velocity electrons and bring the current balance to zero. The fraction of ambient electron current repelled is:

$$J_{es} = J_{eo} \exp\left(-\left|q\phi\right|/kT_e\right) \ , \tag{4}$$

where

ϕ = satellite potential,
q = charge on electron,
kT_e = electron energy (thermal),
J_{es} = electron current to spacecraft,
J_{eo} = electron current for 0 satellite potential.

13. Rosen, A. (1975) Spacecraft Charging: Environment Induced Anomalies, Paper 75-91, AIAA 13th Aerospace Sciences Meeting, 1975.

14

Without illumination the current balance becomes:

$$J_{es} = J_i \, , \tag{5}$$

$$\therefore \ \ J_i = J_{eo} \exp(-|q\phi|/kT_e) \, . \tag{6}$$

Assuming approximate equality of the ion and electron energies reduces the current ratio to the particle mass ratio. Solving for the satellite potential:

$$\phi = \frac{-kT_e}{q} \ln \frac{J_{eo}}{J_i} = -3.7 \frac{kT_e}{q} \, . \tag{7}$$

Thus, during eclipse, if the satellite is immersed in an energetic, kilovolt electron plasma, as is often the case during magnetic storms, the satellite surface potential will be driven thousands of volts negative.

During periods of illumination, the photoelectron and the ambient electron currents will so dominate the ion current that the current balance equation will effectively reduct to:

$$J_e = J_{ph} \, , \tag{8}$$

$$\phi = \frac{-kT_e}{q} \ln \left(\frac{J_{eo}}{J_{ph}} \right) \, . \tag{9}$$

The average electron temperature will be dominated by the more numerous photoelectrons. Since the photoelectrons characteristically have energies of a few electron volts, no matter which electron current dominates, the satellite potential will remain at a few volts negative or positive. It would only be under severely disturbed conditions when $J_e \gg J_{ph}$ that negative potentials of a hundred volts or higher could be expected. Under normal conditions the photoelectron current dominates and a slightly positive potential exists on the spacecraft.

Representative values of the currents and particle energies to be encountered at synchronous orbit are given in Table 1. Although they are only approximate (several effects, like secondary and backscattered electrons and the satellite sheath, are ignored), one can utilize the two simple equations:

$$\phi_{\text{illuminated}} = \frac{-kT_e}{q} \ln (J_{eo}/J_{ph}), \tag{10}$$

and

15

$$\phi_{eclipse} = \frac{-kT_e}{q} \ln (J_{eo}/J_i) \,, \tag{11}$$

and the data presented in Table 1 or in the following sections of this report, to approximately compute satellite potentials. Keeping in mind the fact that the currents are related to the product of the density and velocity, the response of the potential to various synchronous orbit conditions can be effectively analyzed through studying variations in this product.

Table 1. Representative Values of Currents and Particle Energies to be Encountered at Synchronous Orbit

(50 eV < E < 80 keV)		Maximum	"Typical"	Minimum
I.	Electrons (Omnidirectional)			
	A. Number Density (particles/cm^3)	8	1	0.01
	B. Mean Energy (keV)	50	16	0.1
	C. Number Flux (10^6 particles/cm^2-sec-ster)	1500	150	2
	D. Energy Flux (erg/cm^2-sec-ster)	16	1.5	0.1
	E. Current (nA/cm^2)			
	Ambient:	4	0.2	0.02
	**Photoelectron:	4	2	0.8*
	**Secondary + Backscattered:	0.8	0.2	0.016
II.	Ions (Omnidirectional)			
	A. Number Density (particles/cm^3)	4	1	0.03
	B. Mean Energy (keV)	60	12	0.1
	C. Number Flux (10^6 particles/cm^2-sec-ster)	25	10	2
	D. Energy Flux (erg/cm^2-sec-ster)	0.9	0.3	0.05
	E. Current (nA/cm^2)	0.02	0.01	0.005

*Eclipse = 0

**"Best estimate" as very material dependent

3.2 Spacecraft Potential Variations When Illuminated

In the previous section, the role of the photoelectron flux in determining spacecraft potential was described. Ignoring for the moment the effects of differential charging and satellite structure, satellite charging under the influence of photoelectron fluxes can be divided into two cases. Either the photoelectron flux leaving the spacecraft dominates, in which case a positive potential of a few volts is observed,

16

or the ambient electron flux dominates, in which case a negative potential is reached. For the latter case, maximum potentials of about -200 V were observed[4] on ATS-5 while for ATS-6 approximately 10 percent of the observed charging events were greater than -200 V.[6] In one example the potential reached -2200 V on ATS-6.[6]

The ATS-6 spectrogram of Figure 3 (Day 81, 1976) and the accompanying distribution function vs energy profile for 2101 UT in Figure 4 show a period in which a very low intensity ambient flux and a photoelectron background (the eclipse
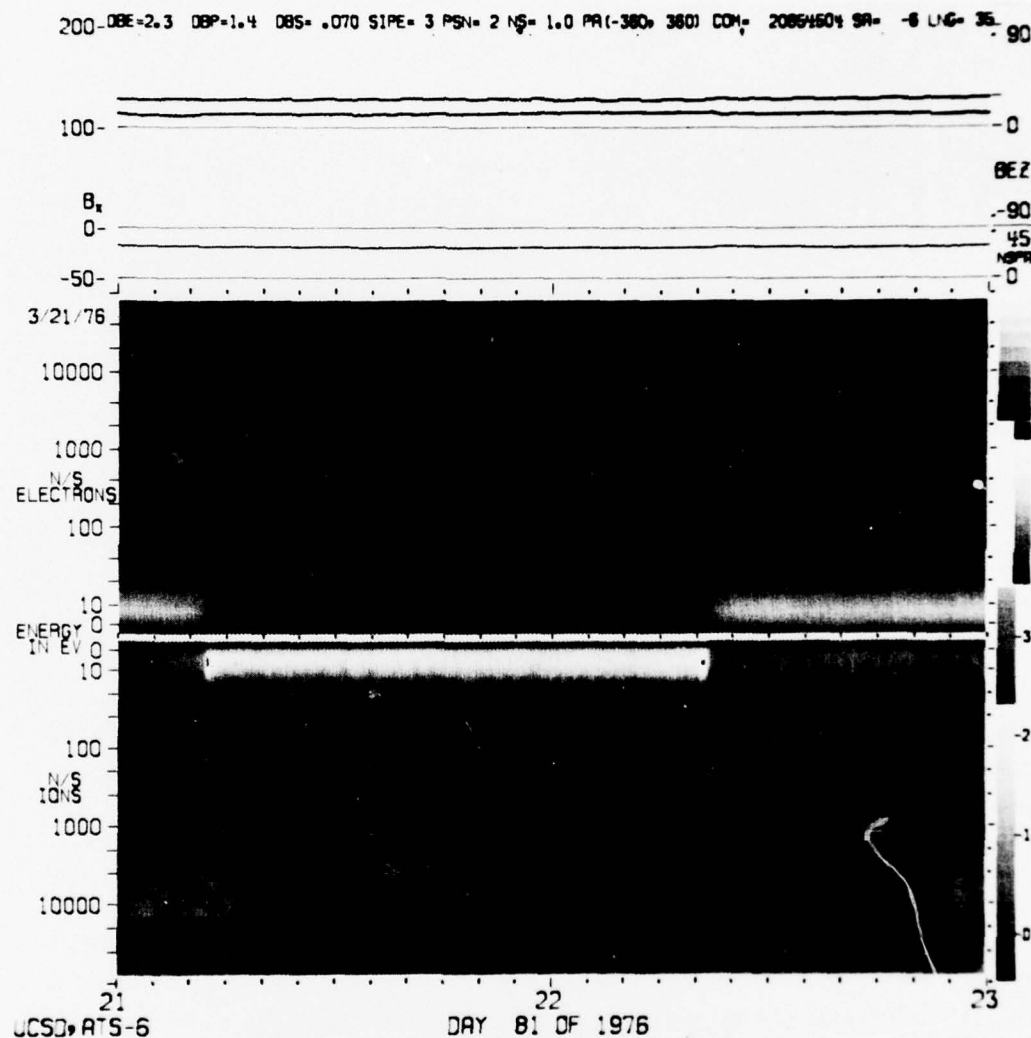
Figure 3. A Spectrogram of Plasma Conditions Observed by ATS-6 on Day 81, 1976, Between 2100 and 2300 UT. (See Deforest and McIlwain[14] for an explanation of the spectrogram format.) Local midnight occurs at 2145 UT. An eclipse occurs between 2110 and 2220 UT. The spacecraft potential varies from slight positive to -10 V

17
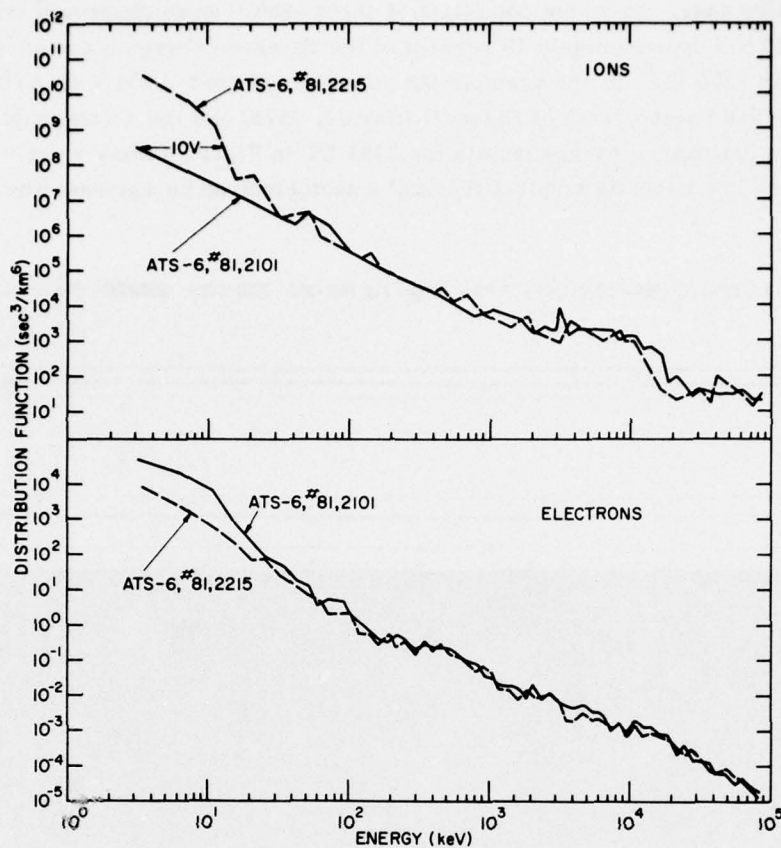
Figure 4. Distribution Functions for the Ions and Electrons
Observed by ATS-6 on Day 81, 1976, at 2101 and 2215 UT

interval between 2010 UT and 2220 UT will be discussed later) were observed. The fact that we see a photoelectron background at all is an indication that, barring possible differential charging or sheath effects, the spacecraft has a slight positive potential. The electron spectrum at 2101 UT has two parts - a weak, ~5 keV component and a photoelectron component (although it is impossible to completely separate secondary and backscattered electrons from photoelectrons, study of the distribution function when the spacecraft is in eclipse at 2215 UT indicates that these fluxes are only about 10 percent of the photoelectron flux). The positive ion flux consists of the high energy remnants of an injection event (that is, weak ring current). As a result, the photoelectron flux is a significant percentage of the total flux to the spacecraft. Thus, the spacecraft becomes charged to a few volts positive since the flux of positive ions to and photoelectrons from the spacecraft is greater than the incident electron flux.

18

In contrast to the preceding event, the event shown in the ATS-6 spectrogram of Figure 5 and the distribution function vs energy spectra of Figure 6 indicate large negative potential variations on the spacecraft. The data were taken during a very active period (K_p was 6+) and illustrate the effects of an intense incident flux when the satellite is illuminated. The spectrum in Figure 6 at 0304 UT covers an active period prior to the charging event. The electron temperature is about 2.8 keV and the density 0.81 cm^{-3} (50 eV to 80 keV). Referring to Figure 5, it would appear
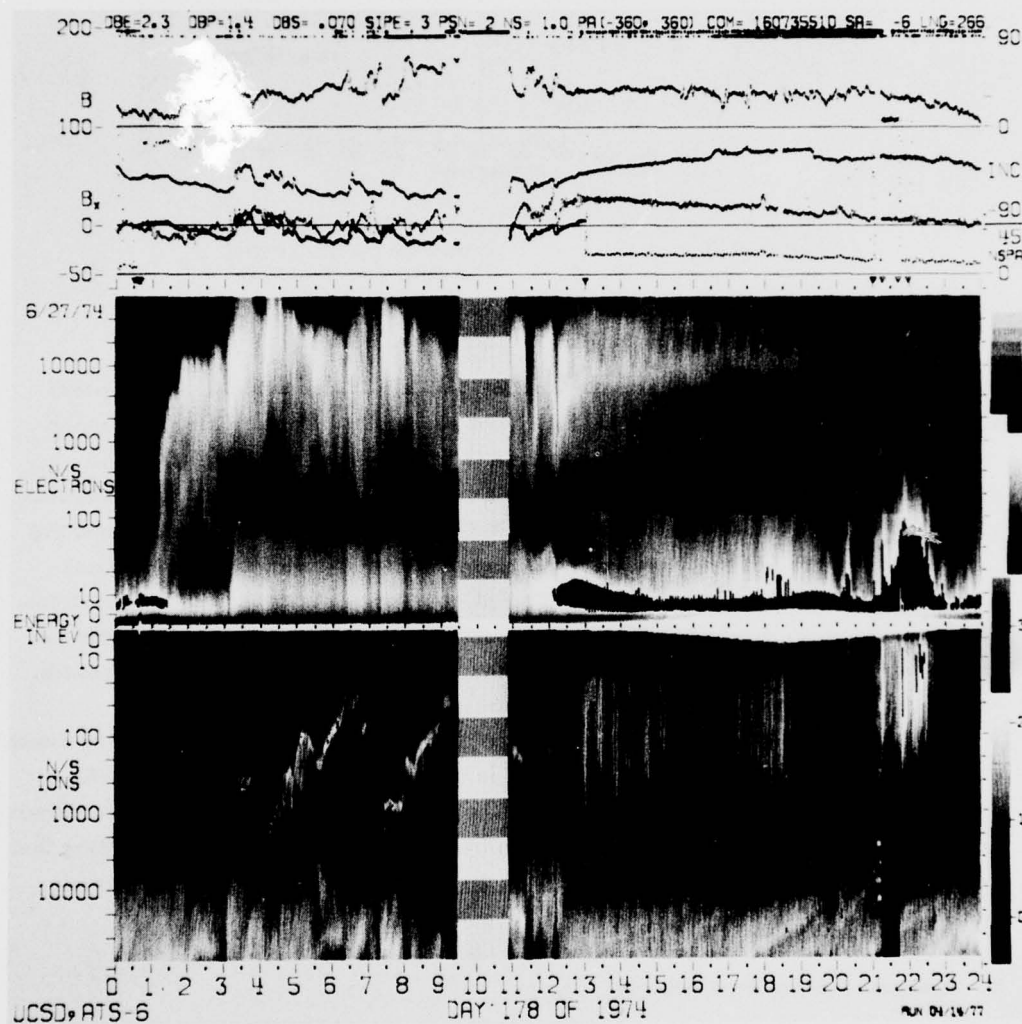
Figure 5. ATS-6 Spectrogram for a Particularly Active Day (K_p of 6+) When Negative Potential Variations of Over 1000 V Were Observed

19
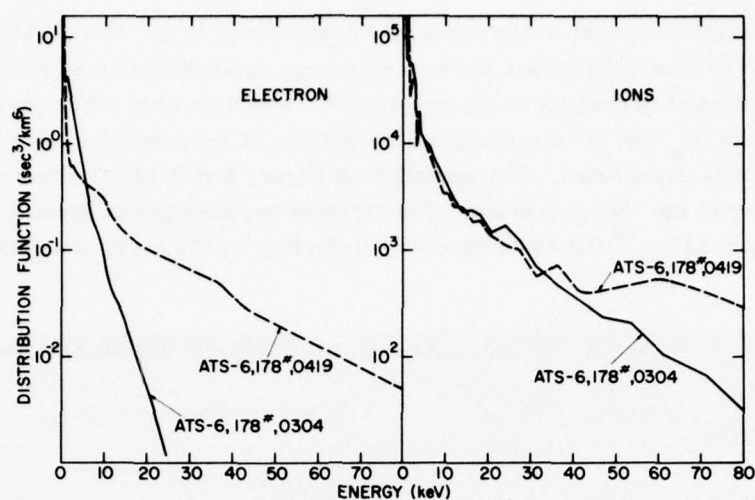
Figure 6. Distribution Functions for Electrons and Ions Observed During the Period of Intense Geomagnetic Activity Shown in Figure 5. The data are from 0304 UT and 0419 UT on Day 178, 1974

from the magnetic and particle records that, at 0315 UT and 0400 UT, compressions of the magnetosphere took place. This caused an intensification of the particle fluxes and an increase in temperature (that is, an injection event). The spectrum at 0419 UT, Figure 6, indicates a temperature of 17.8 keV and densities of 1.10 cm^{-3}. Thus, in the interval 0300 UT to 0419 UT, the balance between the incident electrons and the positive ions, photoelectrons, secondaries, and backscattered electrons was significantly altered resulting in large potential variations. The negative voltage reached only 1600 V and not a much higher value because of the photoelectrons. During an eclipse, when the photoelectrons would not be present, potentials as high as 18,000 V would have been observed.

It should be noted that the potential varies greatly over the lifetime of the event, changing by hundreds of volts on time scales of a minute or less. The ATS-6 instrument returns a complete spectrum only every 16 seconds. Between successive spectra the potential is observed to change by several hundred volts, indicating that the time scale for significant variations in the potential must be on the order of seconds.

3.3 Spacecraft Potential When in Eclipse

As a satellite passes into eclipse, the flux of photoelectrons disappears. The simple theory presented earlier predicts that, since a major source of negative

20

charge leaving the spacecraft has been eliminated, the spacecraft can reach high potentials representative of the ambient electron temperature. The final voltage is, in actuality, a complex function of the flux of incident electrons and ions as well as the flux of backscattered and secondary electrons. In fact, one third of the eclipses studied during the ATS-6, 1976 spring eclipse season exhibited no noticeable charging—the incident electron flux was too low in temperature and density to significantly perturb the satellite potential. In this section we will present examples first of a period in which no charging was observed, next a period of very weak charging, and finally one example of intense charging.

The ATS-6 spectrogram, Figure 7, is representative of a quiet period. The spacecraft is in a region of an intense positive ion ring current. An eclipse takes place at 2126 UT and lasts until 2217 UT. During the entire event there is no noticeable change in the particle spectra outside of a loss of photoelectrons. This figure should be compared with Figure 3. The major difference in these two periods is the presence of a much more intense ion component in Figure 7. This component, by itself, apparently keeps the spacecraft near 0 potential. In Figure 3, however, the loss of photoelectrons on entry into eclipse is sufficient to allow the ambient electron flux to dominate and charge the spacecraft slightly negative (-10 V). In Figure 4, spectra from before and after the eclipse are compared.

ATS-6 data, for an interval of pronounced charging during an eclipse, are given in Figure 8. The distribution functions preceding and during the eclipse are given in Figure 9. We have computed the distribution functions for the electrons and ions to illustrate how the distribution function is not changed when the satellite is eclipsed but rather raised by about 8000 eV in energy for positive ions and lowered by 8000 eV in energy for the electrons. This effect can most easily be explained by assuming the spacecraft to be charged negatively by about 8000 V. By far the most significant feature of this event is the intense incident electron flux which has a temperature of about 8.8 keV. This flux is the dominant factor in establishing the potential of the spacecraft which is, as predicted by the simple theory, near the temperature of the electrons. It is again important to note that this potential is by no means constant over the course of the eclipse. For this case the potential varies between approximately 6 kV and 15 kV during the eclipse with significant changes taking place on time scales of a minute. Such rapid variations in potential place great electrical stress on the surface materials of the satellite and are probably a prime contributor to the operational difficulties encountered by satellites during eclipses.
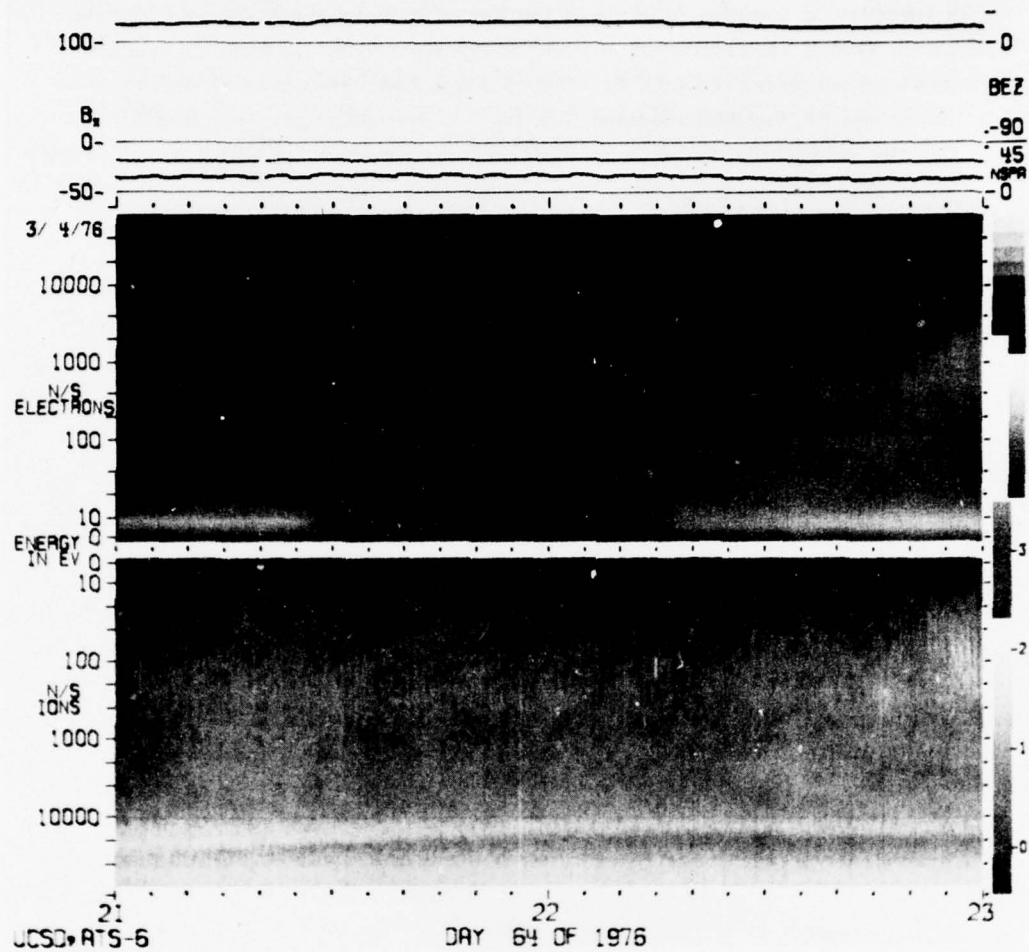
Figure 7. ATS-6 Spectrogram of a Quiet Day. Only weak electron fluxes and a high energy ion flux were observed. The photoelectrons observed between about 5 to 12 V are probably trapped by a differential charging barrier. An eclipse occurred between 2127 and 2217 UT

22
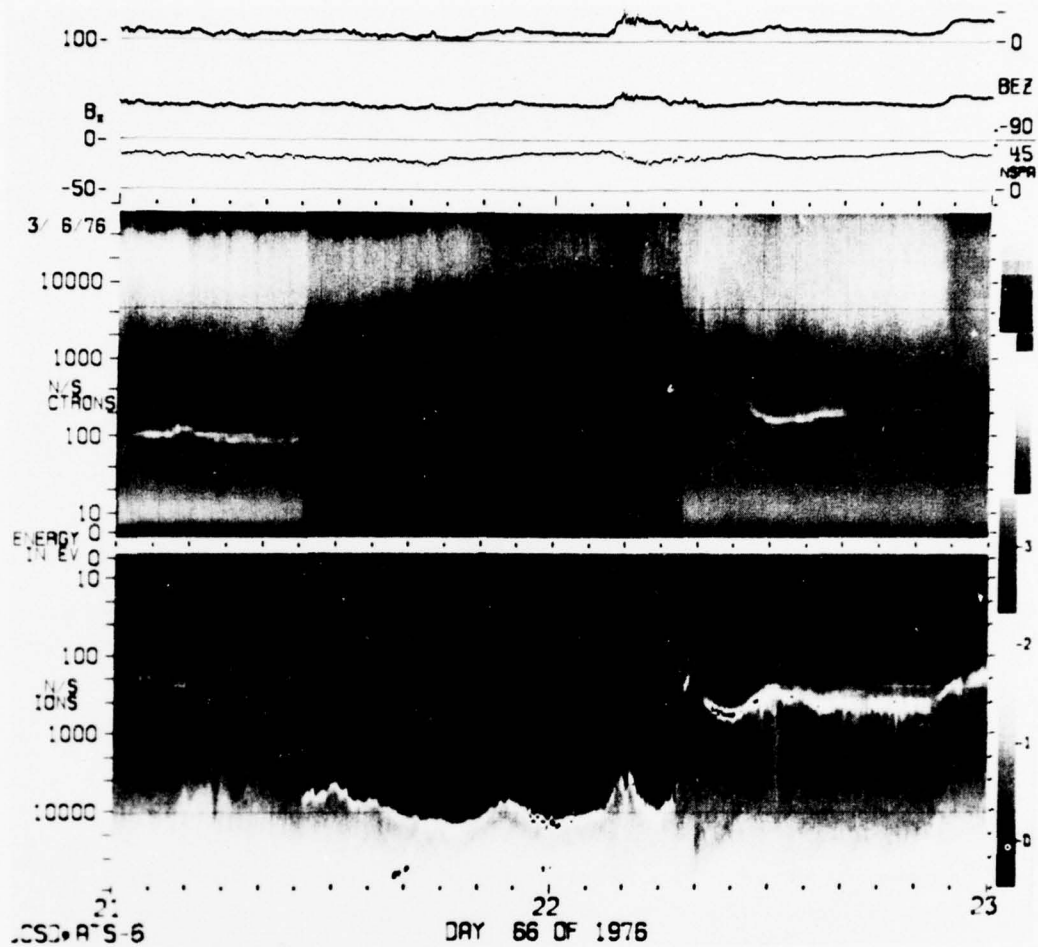
Figure 8. ATS-6 Spectrogram for a Satellite Eclipse on Day 66 of the 1976
Spring Eclipse Season. The spacecraft had a potential of -200 V prior to the
eclipse and reached about -15, 000 V during the eclipse

23
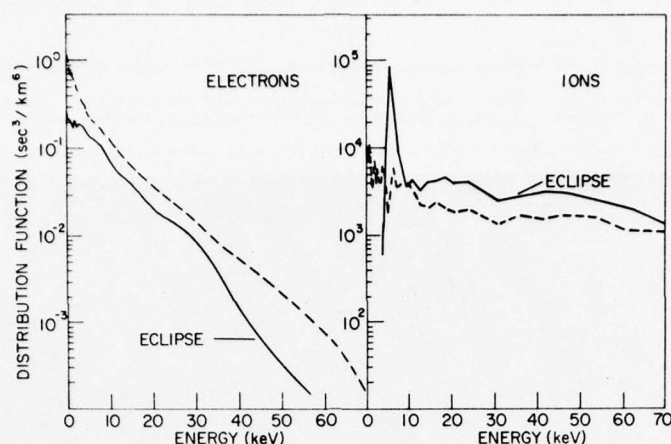
Figure 9. Distribution Functions for the Ions and Electrons for 2123 UT (before eclipse) and 2127 UT (during eclipse) for Day 66, 1976. The apparent displacements between the two sets of distribution functions are attributable to a change of approximately -8000 V in spacecraft potential upon entry into eclipse

4. SATELLITE POTENTIAL VARIATIONS – TIME DEPENDENT

4.1 Theory

The method of computer simulation of a plasma is a new and powerful technique for understanding time variations in a plasma. By simulating a plasma with thousands of computer particles which are moving in response to the forces in a plasma, insight can be gained into plasma time variation problems which are not, in general, analytically tractable.

The basic case of an idealized sphere has been simulated by Rothwell et al. [9] Particular emphasis has been given to the problem of determining the time constant for a satellite to reach its steady-state floating potential for a given plasma temperature and density. Even for the low densities found at synchronous orbit, simulations using every particle would require an excessive amount of computer time. It is fortunate, however, that through scaling, computer simulations which work with higher density plasmas can be applied to plasma having a density of $1/cm^3$ and electron temperatures of 5 keV (values which are characteristic of geosynchronous orbit).

In Langmuir theory, the floating potential of a spherical probe is independent of density. The current is, however, directly proportional to density so that the rate of charge buildup is directly proportional to the density. From this it is clear that

24

the time scale for a satellite to accumulate charge should be inversely proportional to density.

The computer simulation results in Figure 10 show the simulated time response for plasma conditions corresponding to a density of $8 \times 10^4/cm^3$; an electron temperature of 5 keV and an electron to ion temperature ratio of 0.5. Under these conditions the satellite is able to reach equilibrium in about 6 μsec. In this figure the data points represent the output of the simulation code, while the spread in data points is representative of computer and plasma noise inherent in the simulation technique. The final potential shows good agreement with the Langmuir theory which predicted a potential of 12.9 keV.
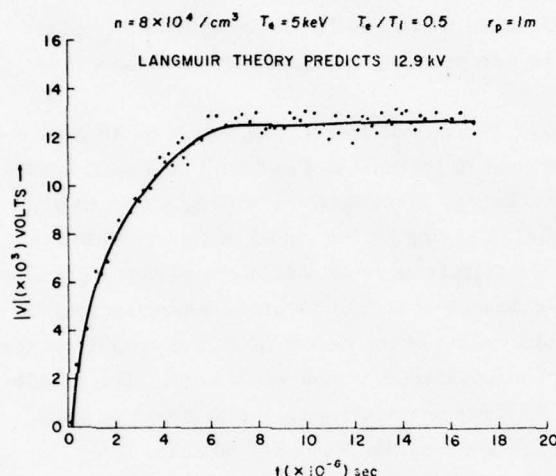
Figure 10. Computer Simulated Model of Potential Variations on a Spherical Spacecraft. The points represent the actual data while the line is a smoothed fit. The fluctuations are due to plasma oscillations and numerical oscillations inherent in the simulation technique

Scaling the results of Figure 10 by the ratio of the model density to a density of $1/cm^3$, which is more representative of geosynchronous orbit, gives a time constant of 0.4 sec. This then should be the characteristic time scale for satellite charging and should be kept in mind in subsequent discussions. Unfortunately, the maximum time resolution possible from ATS-5 and ATS-6 is roughly 0.5 sec. In the following sections, examples of potential variations on the order of hours (differential charging), minutes (Alfven waves), and seconds (ion cyclotron frequency) will be presented for comparison with theories such as the one just outlined.

4.2 Time Variations — Observations

In previous sections, general types of charging phenomena were discussed with the purpose of demonstrating how different ambient plasma parameters altered the potential of the spacecraft. In this section examples of the effects of rapidly varying

25

these parameters will be studied. Evidence for differential charging from both ATS-5 and ATS-6 will be discussed. Examples of increases in the potential, as the spacecraft pass into eclipse, will demonstrate the effects of rapid changes in the photoelectron current. Substorm injection events, when the particle population is changing in minutes or less, will be presented to show how rapidly the satellite potential can response to plasma variations. These examples will provide a qualitative if not quantitative understanding of the time variations to be encountered by a spacecraft.

4.2.1   DIFFERENTIAL CHARGING

Probably the major cause of difficulty due to charging of spacecraft is differential charging—the charging of different portions of the spacecraft to different potentials. Unfortunately, differential charging is a difficult phenomenon to study with the data now available. At best we can present examples and show how they affect spacecraft behaviors.

Figure 11 is a spectrogram of data taken parallel to the spin axis on 30 November 1969 for ATS-5.[5] The feathered pattern in the ions is the result of a spin modulation of the data. The cutoff in the low energy electrons, indicating a negative potential (~1000 V), points to differential charging as the cause of this modulation. This is supported by the fact that neither feature is observed in the sensors perpendicular to the spin axis. A possible source of this differential charging may be the buildup of charge (due perhaps to shadowing of the detector) in the vicinity of the parallel detector (see DeForest[5] from which this example was taken). The resulting electric field would then cause an $\overline{E} \times \overline{B}$ force when coupled with satellite spin and the local magnetic fields that could reproduce the feathered pattern.

Figure 12, also from DeForest,[5] is an ATS-5 spectrogram of data taken parallel to the spin axis on 16 October 1969. The apparent charging commencing at 0600 UT is not observed on the perpendicular detector indicating a differential charging event. The event decays within 20 minutes of the beginning of the eclipse at 0630 UT and builds up again at the same rate following the eclipse giving some indication of the time scales involved in charging different surfaces on the satellite. The variety of materials and shadowing problems encountered on satellites casts doubt on the usefulness of using this time constant but it does serve as an estimate of the magnitude.

Figure 8 which was used as an example of eclipse charging, also exhibits evidence of differential charging on the ATS-6 satellite. In the period immediately before and after the eclipse, there is approximately a 200 V negative potential on the spacecraft. Note, however, that there are significant electron fluxes present below this voltage. Whipple[8] has attempted to explain this effect in terms of a sheath potential barrier around the spacecraft which would trap the electrons in

26
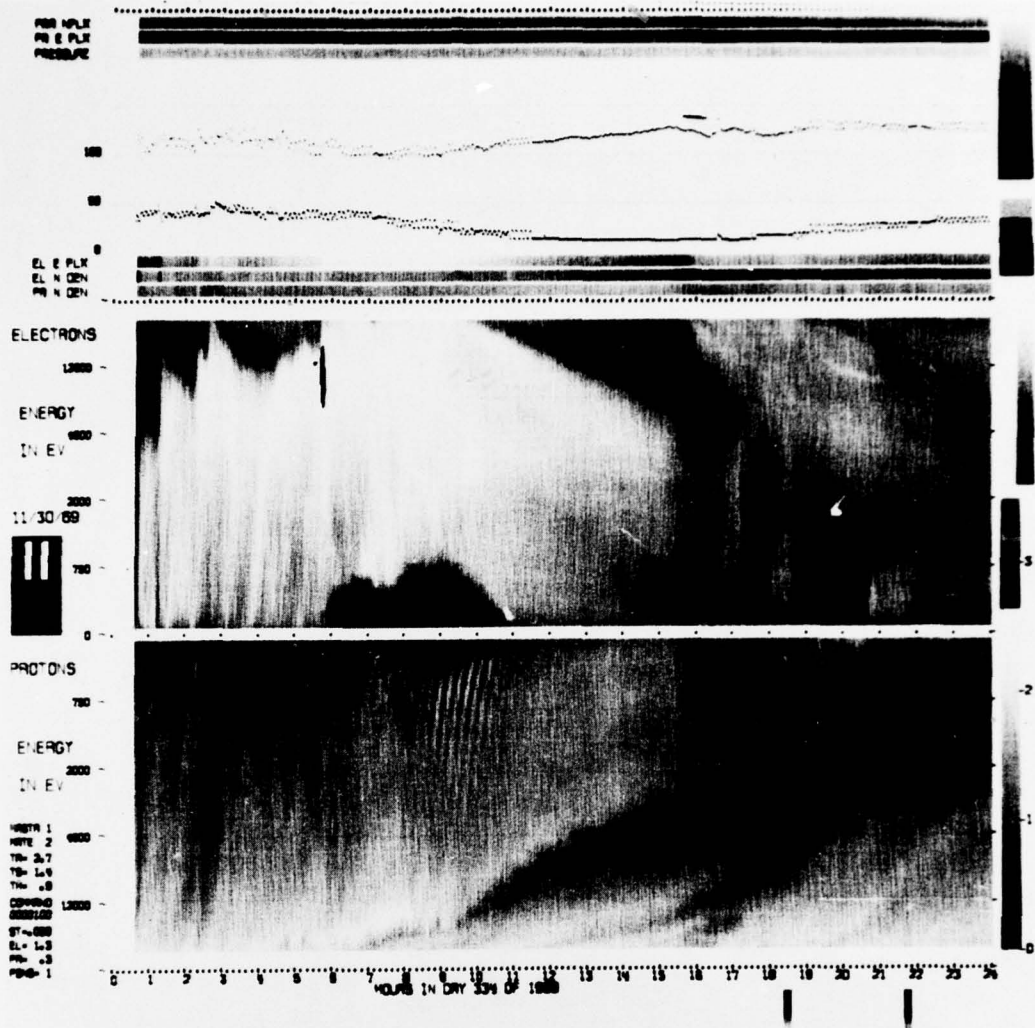
Figure 11. Day 334, 1969, Spectrogram From ATS-5. The feathered pattern in the ions between 0700 and 1100 UT and the corresponding loss of low energy of electrons is real and the result of differential charging[5]

the vicinity of the satellite. His calculations indicate, however, that such a barrier would not be adequate to contain the observed fluxes. He suggests, therefore, that differential charging, such as might be produced by charge buildup on the large antenna in front of the particle detectors, may be the cause of these variations.

In concluding this brief description of differential charging, a further problem remains to be addressed. For a rotating or spinning satellite the problem of
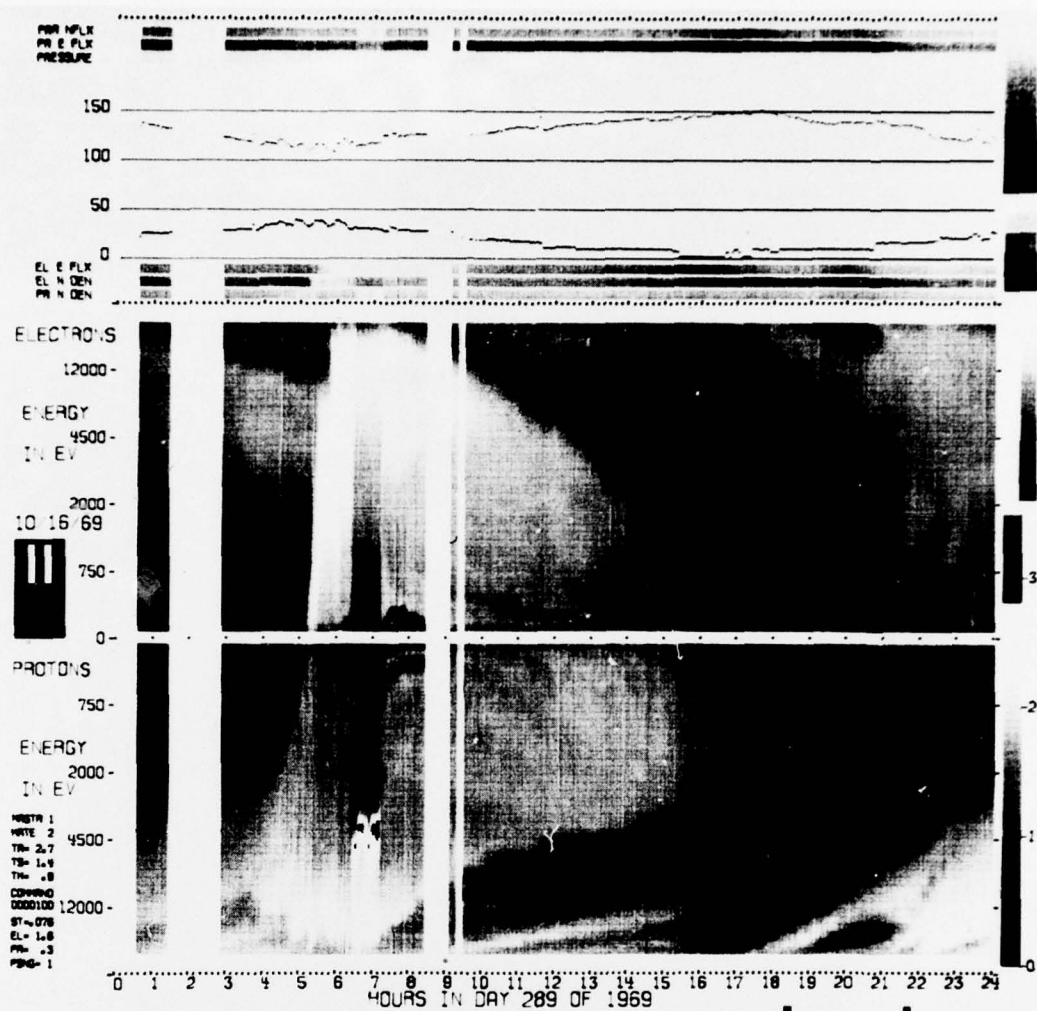
Figure 12. Day 289, 1969, Spectrogram From ATS-5 Which Exhibits the Buildup (during an injection event) and Decay (during eclipse) of Differential Charge on the Satellite

differential charging is complicated by the fact that the regions of the satellite that are illuminated or shadowed will be varying as a function of time as the satellite spins. For such a case, we expect differential charging phenomena to be taking place on the time scale of the spin period or less. This phenomenon, which has not yet been observed, is different from that in Figure 11 where a static field near the sensor is modulating the data. Here the potential on a particular surface element of the satellite would vary as it alternately passes in and out of illumination.

28

4.2.2 INJECTION EVENTS

In the study of geomagnetism much effort has gone into the analysis of what are called geomagnetic storms and substorms. Geomagnetic storms are known to last many days while substorms occur on time scale of an hour or less. Both are closely tied to the auroral displays that affect the polar regions. Perhaps the major advance in understanding these storms in the last two decades has been the discovery that the storm is actually composed of a series of substorms. Substorms are observed as short duration magnetic variations (usually accompanied by large excursions of the horizontal amplitude of the magnetic field at the earth's surface that last from about 20 minutes to 2 hours) coupled with brightening of the aurora near midnight and westward traveling auroral surges.

There are good experimental data that associate substorms with the injection of plasma observed at the geosynchronous orbit. [14] It has long been believed that movements of the plasma sheet earthward, accompanied by intensification of the particle fluxes, are a major aspect of substorm morphology. Although some recent work[15] has tended to play down a close, direct relationship between the movements of the plasma sheet at synchronous orbit and specific substorm features (see, however, Eather et al), [16] the idea of a plasma injection during substorms is still a useful concept. In particular, the major link between satellite malfunctions and spacecraft charging is believed to have been observed during periods of substorm activity[1-3] associated with plasma injection at synchronous orbit.

Figure 13, from ATS-5, is an example of an injection event. Injections occurred at approximately 2300 UT on Day 336, 0100 UT on Day 337, and 0715 on Day 337 of 1970. This is given by the time at which the satellite first encountered the highest energy positive ions. The inner edge of a plasma cloud generated by the event was encountered at 0500 UT on Day 337 of 1970 (the point where electrons and ions are first simultaneously observed). The main part of the cloud is encountered near local midnight (0730 UT). Note the particularly intense and rapid development between 0700 UT and 0720. It is this increase in the electron flux and temperature associated with the plasma injection that leads to large spacecraft potentials.

Figure 14, from ATS-6, is an enlargement in time of the region near midnight. In this event, the satellite was initially immersed in relatively low energy, plasmasphere plasma. The satellite passes into eclipse at 2120 UT, but no charging is observed until 2135 when the satellite encounters a plasma cloud characteristic of

14. DeForest, S. W., and McIlwain, C. E. (1971) Plasma clouds in the magnetosphere, J. Geophys. Res., 76(No. 16):3587-3611.

15. Akasofu, S-I, DeForest, S. E., and McIlwain, C. E. (1974) Auroral displays near the 'foot' of the field lines of the ATS-5 satellite, Planet. Space Sci., 22:25-40.

16. Eather, R. H., Mende, S. B., and Judge, R. S. (1976) Plasma injection at synchronous orbit and spatial and temporal auroral morphology, J. Geophys. Res., 81(No. 16):2806.

Figure 13. ATS-5 Spectrogram for Day 337, 1970, of an Isolated, Pre-midnight Substorm

an injection event (high density, high temperature). The satellite potential, as reflected by the ions, responds rapidly. The rate of voltage change during this event is about 1000 V/min (going from 0 to 5000 V in 5 min). Although probably an underestimate of the maximum response time to an injection during an eclipse, this yields an order of magnitude estimate of the satellite response to injection events.

30
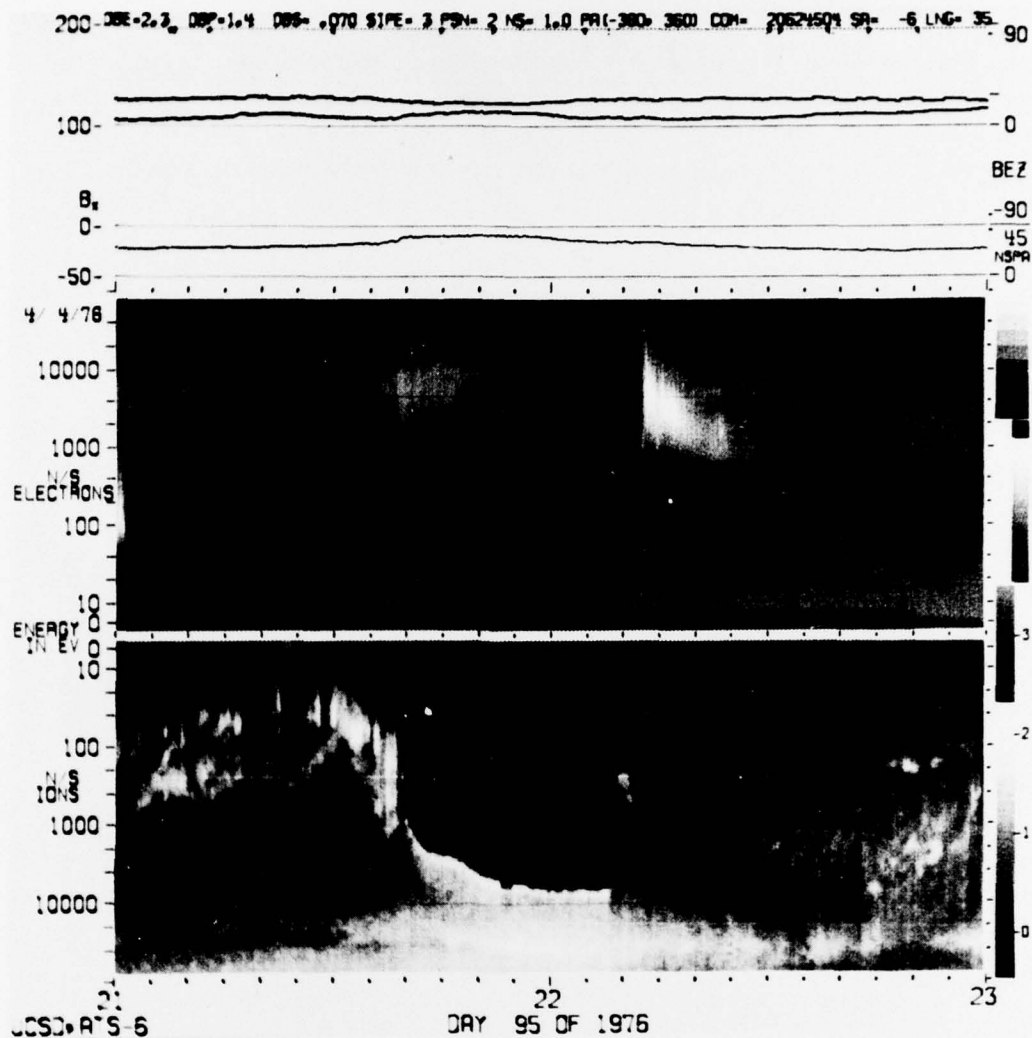
Figure 14.   ATS-6 Spectrogram for the Eclipse on Day 95, 1976, Which Shows an Injection at 2137 UT During the Eclipse.   Note the rapid -10,000 V potential variation following the injection

4.2.3   ECLIPSE VARIATIONS

In the preceding example it was shown how a spacecraft became charged during an eclipse when it encountered a plasma cloud.   This can be compared with the related case of passing into eclipse while immersed in a plasma cloud.   For the latter case, it is possible to study in detail the passage into eclipse concentrating on the

31

penumbral phase of the eclipse when the solar illumination is rapidly varying. Careful examination of the spectrogram in Figure 15 reveals the rapid time variation of the potential as the ATS-6 spacecraft enters and exits eclipse.[17] Note also the symmetry of the event and approximate stability of ambient plasma conditions

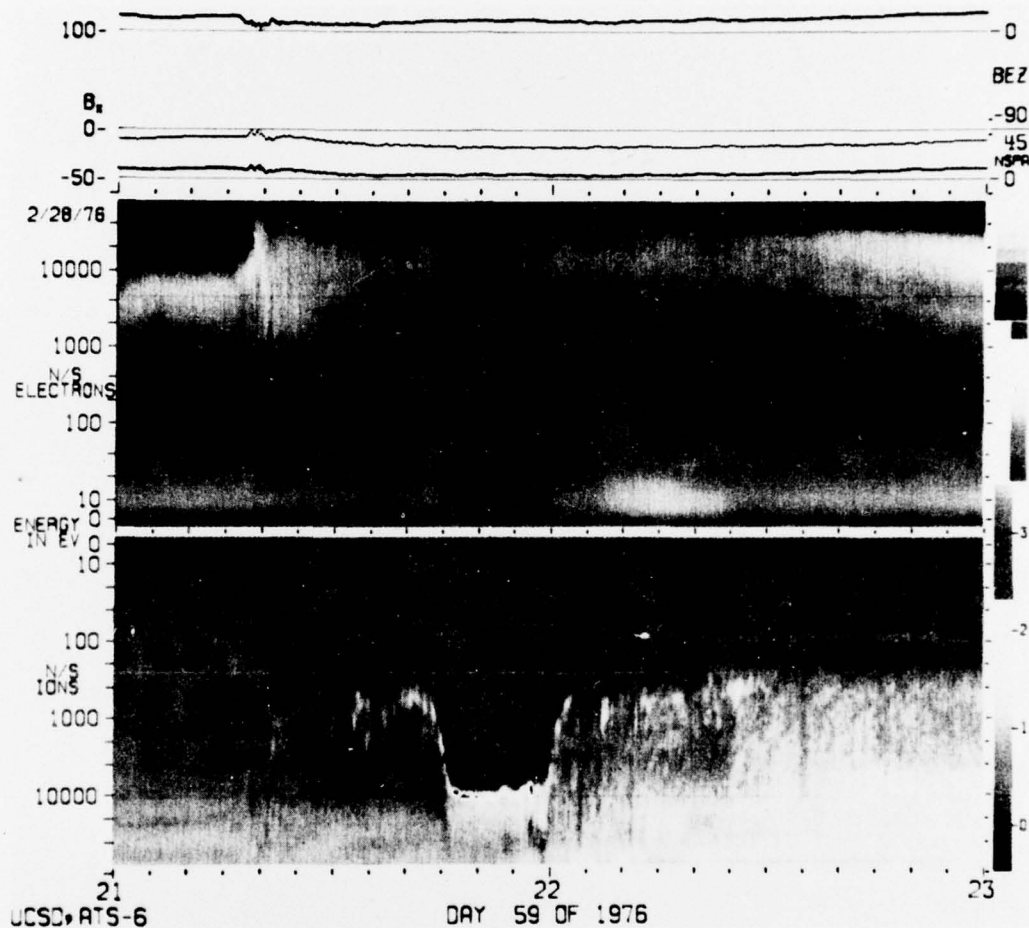Figure 15. ATS-6 Spectrogram for Day 59, 1976. This is the first observed eclipse for the 1976 spring eclipse system. It is near the minimum period possible for an observable total eclipse and, as a result, the satellite spends maximal time in partial eclipse (8 min total)

17. Garrett, H. B. (1977) Analysis of penumbral data from ATS-6, Proc. of the Space Charging Conference, AFGL-TR-77-0051/NASA TMX-73537.

before, during, and after eclipse. For reference, Figure 16 is a plot of the 1976
ATS-6 spring eclipse season during which that eclipse occurs. Where possible the
duration of the eclipses (both penumbral and umbral) have been estimated and com-
pared with a simple model which gives the time of entry into partial and total eclipse
as a function of the day of the year. The duration of partial eclipse for the 1976
spring season ranges from about 1 min to as long as ~5 min (Figure 15) for grazing
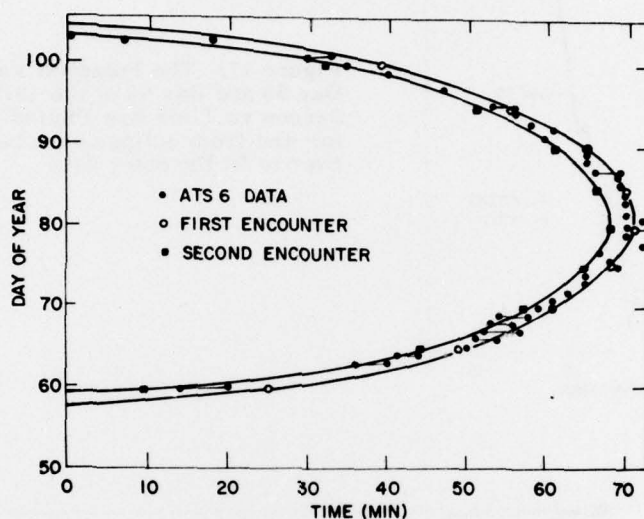incidence.

Figure 16. ATS-6 1976 Spring Eclipse Season Data
Were Studied and the Time the Satellite Spent in Total
and Partial Eclipse Estimated. A simple theory which
predicts eclipse times (squares for total eclipse; open
circles for partial eclipse) for the eclipse season is
compared with the data

The satellite potentials for entry and exit for two days (see Figure 8 and Fig-
ure 15) are plotted in Figure 17 (the exit data have been folded over on the entry
data). A model including atmospheric effects[17] has been derived that gives the
solar illumination vs time as the satellite passes into eclipse. Study of data from
the Injun V satellite confirmed that the solar illumination is directly related to the
photoelectron flux. [17] It is possible to combine the observations in Figure 17 with
the theoretical predictions of the solar illumination/photoelectron flux. This has
been done in Figure 18 which shows the potential vs solar illumination/photoelectron
flux. The fact that the two curves are in reasonable agreement for two different
days (Day 66 is an example of direct incidence whereas Day 59 is an example of

33

grazing incidence) which have different penumbral eclipse durations—1 minute for Day 66 and 4 minutes for Day 59—indicates that the response time of the spacecraft to photoelectron variations is much less than 1 min (that is, the variation on Day 66 was approximately 5000 V in 1 min).
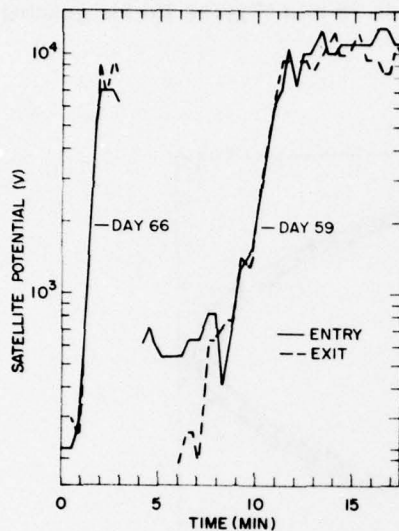
Figure 17. The Potential Variations for Day 59 and Day 66 of the 1976 Eclipse Season vs Time Are Plotted. The data for exit from eclipse have been folded over to fit the entry data
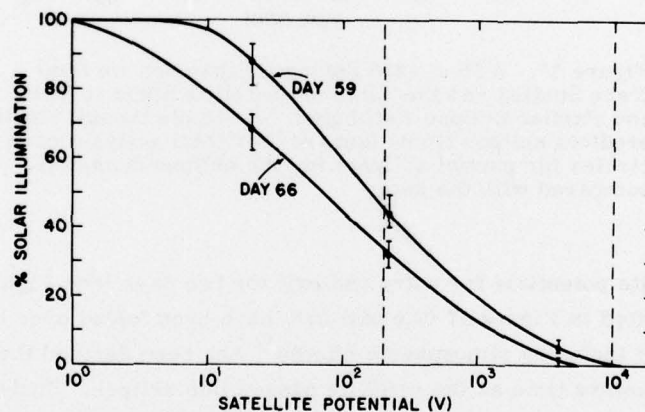
Figure 18. The Percentage of Solar Illumination Falling on ATS-6 Compared With the Potential as the Satellite is Eclipsed. Similarity of the two curves, which correspond to different eclipse conditions, implies that the satellite response is simultaneous over the time ranges considered. The dashed lines represent the region over which the potential values are observed while the error bars correspond to different atmospheric models

34

4.2.4 RAPID TIME VARIATIONS

In the foregoing sections we have seen how the satellite potential can vary significantly on time scales of a minute or less as plasma injection events or eclipses alter the particle population. There are several sources of coherent oscillations in the spacecraft potential on the order of minutes and seconds that also deserve consideration. In fact, such oscillations are seen down to the limit of the ATS-5 and ATS-6 instrumentation (0.32 and 0.25 sec, respectively). The observation of such a continuum in charging variations out to the highest time resolution now available indicates that rapid variations in satellite potential might be a relatively common occurrence.

On at least three occasions (DeForest, private communication) Alfven waves have been observed by ATS-6. Only one, on Day 178 of 1974, will be described here. On that day, coherent oscillations were found in the magnetic field, electron density, and ion density. The ion oscillations were quite pronounced below about 10 keV and had a period of about 2 min. These oscillations were clearly observed for over 2 hours.

Associated with the ion oscillations were potential oscillations on the spacecraft. These oscillations were in phase with the density oscillations—peak values occurring at the same time as peaks in the ion density. A particularly pronounced example of this effect is shown in Figure 19 where the voltage vs time is plotted for a 10-min segment of data. The maximum amplitude is about 18 V (note the -25 V background potential).
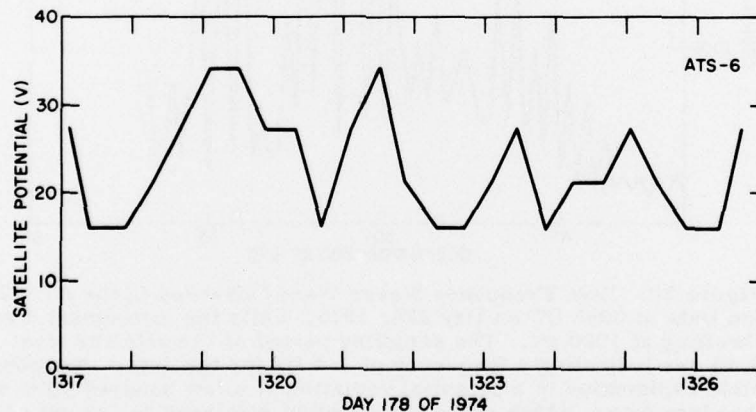

Figure 19. A Plasma Wave, on Day 178, 1974, Was Observed by ATS-6, That Resulted in Satellite Potential Variations. The satellite potential between 1317 and 1326 UT is plotted, demonstrating the oscillations (± 9 V) and the dc offset (-25 V)

35

An even more spectacular event occurred on Day 282 of 1975 at 0037 UT. [18] On this day a particularly fortuitous event occurred. The instrument was dwelling at one energy, 1000 eV, for 16 sec. The satellite was charged to a potential of roughly -1000 V which, by careful examination of spectra immediately before and after the event, oscillated with an amplitude of a few hundred volts. This oscillation modulated the ion count rate as the peak associated with the thermal ion background plasma shifted in and out of the 1000-eV channel (note: the modulation may be explained by a plasma wave rather than charging). Figure 20 illustrates this behavior. The envelope in this figure is clearly modulated. Ignoring aliasing, estimates of the best frequency give a frequency of ~1.4 Hz (the Nyquist frequency for ATS-6 is 2 Hz) for the oscillations. For a 100γ magnetic field the ion cyclotron frequency is approximately 1.59 Hz for protons. Thus, the wave could be tentatively identified as a cyclotron wave for H^+ or some heavier ion (aliasing would mean the wave could have an even higher frequency).
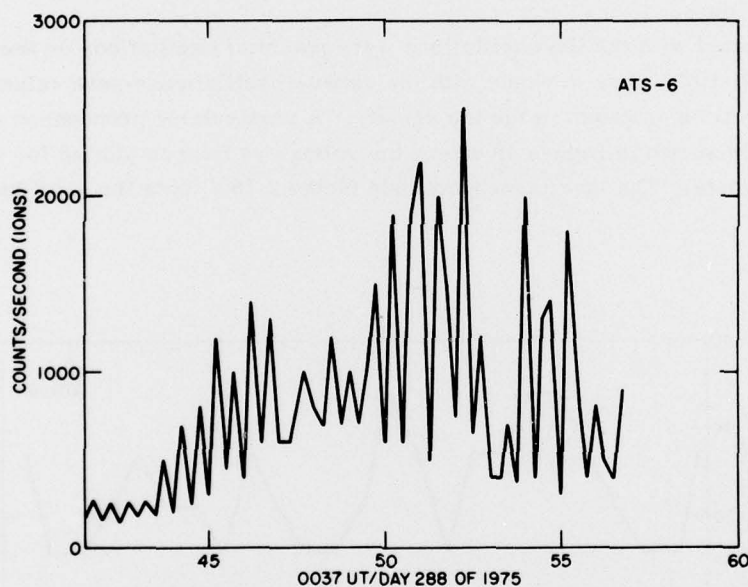
Figure 20. High Frequency Waves Were Observed in the ATS-6 Ion Data at 0037 UT on Day 288, 1975, While the Instrument Was Dwelling at 1000 eV. The sampling period of the satellite was 0.25 sec indicating a frequency of 1.4 Hz for the data. One possible explanation is a potential variation of a few hundred volts at that frequency, which shifts the counting rate peak in and out of the 1000 eV channel

18. DeForest, S.E., and Mauk, R.H. (1976) Modulation of spacecraft potential at the ion cyclotron frequency, EOS, Trans. Amer. Geophys. Union, 57(No. 12).

36

4.2.5 FUTURE POTENTIAL MEASUREMENTS

It has been demonstrated that significant variations in the spacecraft potential take place on time scales of seconds and that such variations pose a serious threat to the proper functioning of the satellite. In order to design future spacecraft to resist the stresses due to spacecraft charging, a greater understanding of rapid potential variations is necessary. To this end the Air Force has designed and will fly aboard the SCATHA (Satellite Charging at High Altitudes) satellite a Rapid Scan Particle Spectrometer which will allow the analysis of variations in the potential occuring on time scales as short as a second or less.

The Rapid Scan Particle Spectrometer consists of two identical sets of detectors; one set arranged parallel to the spin axis of the satellite and the other arranged perpendicular to the spin axis. Both sets of detectors consist of four instruments: a low energy electrostatic analyzer to measure electron and ion fluxes in the energy range from 50 eV to 1.7 keV; a high energy electrostatic analyzer to measure ion and electron fluxes in the energy range from 1.7 keV to 60 keV, a solid state detector to measure the ion flux from 70 keV to 35 MeV, and a solid state detector to measure the electron flux from 30 keV to 1 MeV. In Table 2 we have listed the energy channels for the detectors. The most important feature of this detector is that it will provide a measurement of the ion and electron spectra once each second. Such a high time resolution will permit detailed study of the rapid potential variations. In addition, since the SCATHA satellite will be spinning, the rapid scan capability will allow one to study differential charging as a function of the satellite period.

As an added capability the Rapid Scan Spectrometer can be set to read out any single channel of the detector every 230 μsec. The dwell time in a channel can be set as desired above a minimum dwell time of 200 msec. In the minimum dwell time mode a spectrum over the channels of the electrostatic analyzer can be returned every 8 sec. Such high time resolution should provide valuable information on the potential variations discussed in this paper.

37

Table 2. Energy Channels for AFGL Rapid Scan Particle Spectrometer

Low Energy Electrostatic Analyzer (electrons & protons)	
Channel	Energy range
0	background
1	0. 05 to 0. 12 keV
2	0. 12 to 0. 30 keV
3	0. 30 to 0. 70 keV
4	0. 70 to 1. 70 keV

High Energy Electrostatic Analyzer (electrons & protons)	
Channel	
0	background
1	1. 70 to 4. 20 keV
2	4. 20 to 10. 20 keV
3	10. 20 to 25. 0 keV
4	25. 0 to 60 keV

Solid State Spectrometer (electrons)	
0	30 to 45 keV
1	45 to 70 keV
2	70 to 120 keV
3	120 to 170 keV
4	170 to 243 keV
5	243 to 275 keV
6	275 to 560 keV
7	560 to 10, 000 keV

Solid State Spectrometer (protons)	
0	70 to 100 keV
1	100 to 165 keV
2	165 to 290 keV
3	290 to 450 keV
4	450 to 725 keV
5	725 to 1000 keV
6	1000 to 2400 keV
7	2400 to 6000 keV
8	6000 to 15, 000 keV
9	15, 000 to 35, 000 keV

5. CONCLUSIONS

We have reviewed the ATS-5 and ATS-6 data currently available on spacecraft charging. Particular attention has been placed on the time scale of potential variations. Table 3 summarizes the observed time scales of the various phenomena. This table is based on results reported to date and, as such, is heavily biased towards readily observable, readily interpretable phenomena. It demonstrates, however, the wealth and diversity of spacecraft potential variations already observed.

Table 3.   Observed Time Scales

Event*	Time Scale	Voltage Amplitude (Maximum)
Differential Charging	20 min	± 1 V to ± 1 kV
Injection Event (No eclipse)	~5 min	≤ -2 kV
Injection Event (Eclipse)	~5 min	-20 kV
Eclipse Charging (Penumbral)	1 to 10 min	0 to -20 kV
Alfvén Waves	~2 min	± 10 V
High Frequency Waves (Cyclotron)**	~1 sec	± 100 V

*Note: All values are currently observed upper limits for voltage and lower limits for time.

**May not be a charging event.

Time variations, both coherent and impulsive, in spacecraft potential pose a threat to existing spacecraft systems. These variations, as described, cover a wide range of amplitudes and time scales. It is not difficult to extrapolate the observations of this report and conclude that the time scale of potential variations is a critical component of the spacecraft charging threat. Unfortunately, as Table 3 indicates, there are still rather major gaps in the study of this particular aspect of the charging problem. This is particularly true as we approach short time scales. It is not that rapid time variations have not been observed, but that the observations thus far have been a function of fortuitous instrumental effects. It is to this problem that this paper has been addressed. Plans at AFGL currently call for a high time resolution ion/electron spectrometer to be flown on the SCATHA satellite in early 1979. It is hoped that this instrument will provide significant improvements in our understanding of rapid time variations in spacecraft potential.

1. McPherson, D. A., Cauffman, D. P., Schober, W. (1975) Spacecraft Charging at High Altitudes - The SCATHA Program, AIAA Paper, pp 75-92.

2. Shaw, R. R., Nanevicz, J. E., and Adamo, R. C. (1976) Observations of electrical discharges caused by differential satellite-charging, Spacecraft Charging by Magnetospheric Plasmas, AIAA Progress in Astronautics and Aeronautics Series, Vol. 42, Rosen (Editor).

3. Pike, C., and Bunn, M. H. (1976) A correlation study relating spacecraft anomalies to environmental data, Spacecraft Charging by Magnetospheric Plasma, AIAA Progress in Astronautics and Aeronautics Series, Vol. 42, Rosen (Editor).

4. DeForest, S. E. (1972) Spacecraft charging at synchronous Orbit, J. Geophys. Res., 77:(No. 4):651.

5. DeForest, S. E. (1973) Electrostatic potentials developed by ATS-5, Photon and Particle Interactions with Surfaces in Space, R. J. C. Grard (ed.) D. Reidel Publishing Co., Dordrecht, Holland, pp 263-276.

6. Reasoner, D. L., Lennartsson, W., and Chappell, C. R. (1976) Relationship between ATS-6 spacecraft-charging occurrences and warm plasma encounters, Spacecraft Charging by Magnetospheric Plasmas, AIAA Progress in Astronautics and Aeronautics Series, Vol. 42, Rosen (editor).

7. Parker, L. W. (1976) Theory of electron emission effects in symmetric probe and spacecraft sheaths, Final report (1 Nov 75 - 30 Jun 76), AFGL-TR-76-0294.

8. Whipple, Jr., E. C. (1976) Observation of Photoelectrons and secondary electrons reflected from a potential barrier in the vicinity of ATS-6, J. Geophys. Res., 81(No. 4):715.

9. Rothwell, P. L., Rubin, A. G., Pavel, A. L., and Katz, L. (1976) Simulation of the plasma sheath surrounding a charged spacecraft, Spacecraft Charging by Magnetospheric Plasmas, AIAA Progress in Astronautics and Aeronautics Series, Vol. 42, Rosen (Editor).

10. Frank, L. A. (1971) On the relationship of the plasma sheet, ring current, trapping boundary, and plasmapause near the magnetic equator and local midnight, J. Geophys. Res., 76:(No. 10):2265.

11. Gringauz, K. I. (1969) Low energy plasma in the earth's magnetosphere, Rev. Geophys., 7(No. 1,2):339.

12. Hones, M. E., Jr. (1972) Plasma sheet variation during substorms, Planet. Space Sci., 20(No. 9):1409.

13. Rosen, A. (1975) Spacecraft Charging: Environment Induced Anomalies, Paper 75-91, AIAA 13th Aerospace Sciences Meeting, 1975.

14. DeForest, S. W., and McIlwain, C. E. (1971) Plasma clouds in the magnetosphere, J. Geophys. Res., 76(No. 16):3587-3611.

15. Akasofu, S-I, DeForest, S. E., and McIlwain, C. E. (1974) Auroral displays near the 'foot' of the field lines of the ATS-5 satellite, Planet. Space Sci., 22:25-40.

16. Eather, R. H., Mende, S. B., and Judge, R. S. (1976) Plasma injection at synchronous orbit and spatial and temporal auroral morphology, J. Geophys. Res., 81(No. 16):2806.

17. Garrett, H. B. (1977) Analysis of penumbral data from ATS-6, Proc. of the Space Charging Conference, AFGL-TR-77-0051/NASA TMX-73537.

18. DeForest, S. E., and Mauk, R. H. (1976) Modulation of spacecraft potential at the ion cyclotron frequency, EOS, Trans. Amer. Geophys. Union, 57(No. 12).